PCCP

Accepted Manuscript

ROYAL SOCIETY OF CHEMISTRY

www.rsc.org/pccp

Physical Chemistry Chemical Physics

ARTICLE

Cerium Oxide as a Promoter for the Electro-Oxidation Reaction of Ethanol: In-situ XAFS Characterization of the Pt Nanoparticles Supported on CeO2 Nanoparticles and Nanorods

Received 00th January 20xx,
Accepted 00th January 20xx

DOI: 10.1039/x0xx00000x
www.rsc.org/

Juan Corchado-García[1], Luis E.Betancourt[1], Carlos A. Vélez[1], Sanjaya D. Senanayake[2], Dario Stacchiola[2], Kotaro Sasaki[2], Maxime J-F Guinel[1], Yunyun Zhou[3], Chin Li Cheung[3] and Carlos R. Cabrera[1]*

In this study we probe the electrocatalytic activity of Pt nanoparticles supported on ceria nanoparticles (NP) and nanorods (NR) in the ethanol oxidation reaction (EOR) in alkaline media. The goal of the study was to relate morphology and support structure and composition to the EOR catalytic activity by using in-situ X-ray absorption fine structure (XAFS) studies. Cyclic Voltammetry experiments showed that both ceria supported catalysts (NP vs NR) had similar peak current densities at fast scan rates, however at slow scan rates, the ceria NR catalyst showed superior catalytic activity. In-situ XAFS studies in KOH showed that both ceria supported catalysts had more electron density in their d-band (with the ceria NR having more electron density overall) than the ceria - free Pt/Vulcan standard. However, in an ethanol solution the ceria NR catalyst had the least electron density. We propose that this change is due to the increased charge transfer efficiency between the ceria nanorod support and platinum. In the KOH solution, the increased electron density makes the platinum less electrophilic and hinders Pt-OH bond formation. In the EtOH solution, platinum's increased nucleophilicity facilitates the bond formation between Pt and the electron deficient carbon in ethanol which in turn withdraws the electron density from platinum and increases the white line intensity as observed in the XAS measurements.

A. Introduction

During the past several decades, the ever increasing demands worldwide for energy have been answered with supply from both fossil fuel and renewable energy based technological alternatives to more traditional industrial processes.[1] Of these catalytic reactions that rely on noble-metal (Pt, Rh, Pd, Ru, Ir)[2-6] based catalysts have advanced considerably by providing the best routes to generate electrical and chemical energy. As one such example, alcohol fuel cells are able to convert the chemical energy within molecular bonds of a liquid fuel to electrical energy spontaneously in a highly efficient manner through the use of a catalyst which lowers the energy barrier for the most critical reaction steps. Fuel cell catalysts have become the chief protagonists in the engineering and fabrication of new technologies that rely on such cells as the primary source of energy; however, obstacles remain to improve the efficiency and stability of fuel cell catalysts and in the use for a broader range of commercial and industrial applications. The chemical composition, structure and electronic fingerprint of the catalyst are the key to control and sustain the catalytic activity of the catalyst in an electrochemical reaction, thus obtaining such information from a working catalyst is an imperative. Furthermore, synthetic routes to engineer structure-controlled catalysts play a critical role to regulate size, orientation and morphology of a catalyst in order to achieve simultaneously high activity, selectivity and stability towards alcohol oxidation.

Platinum has been the benchmark catalyst for fuel cell applications for several decades due to its essential physical, chemical and electronic properties that are thought of as the active component essential for this reaction.[2] These attributes and their effect on the electrochemistry have been studied extensively by different spectroscopic techniques including X-ray based methods such as X- Ray Absorption Spectroscopy (XAFS), X-Ray Photoelectron Spectroscopy (XPS) and X-Ray Diffraction (XRD).[7-9]

It has been suggested that rare earth oxides such as ceria (cerium oxide) may be used as a co-catalyst with platinum because of their enhanced ability in adsorbing, dissociating and releasing oxygen via the Ce^{4+}/Ce^{3+} redox cycle. For this reason catalyst based on ceria are very promising for low temperature CO oxidation, WGS and other redox and oxygen reliant reactions.[10-12] Recent work from Cheung et.al. demonstrated the importance of the morphology of the Pt support by comparing the catalytic activity for different nanostructures of ceria supporting platinum nanoparticles, specifically ceria nanorods (NR) with a diameter of 5 to 10 nm and length of 15 to 50 nm as well as ceria nanoparticles (NP) with diameters of 2 to 5 nm. The introduction of oxides to an electro-catalytic system can provide additional structural defect sites without affecting the robustness of the framework, while also providing a reservoir of oxygen. For instance in ceria itself as an electron rich material (4f) is also likely to be an important source of electrons necessary for transfer processes, originating from active centers rich in localized electrons.

[a.1] *Department of Chemistry, NASA-MIRO Center for Advanced Nanoscale Materials, University of Puerto Rico, San Juan, Puerto Rico 00931*
[b.2] *Chemistry Department, Brookhaven National Laboratory, Upton, New York 11973*
[c.3] *Department of Chemistry, University of Nebraska-Lincoln, Lincoln, Nebraska 68588*

In this work, the morphology and support were evaluated for the EtOH electrochemical oxidation with different supports and morphological structures monitored through the use of several advanced in situ and ex-situ spectroscopic technique such as XAFS and XRD. By applying a difference in potential to the solution and monitoring the behavior of the catalyst, the active role of Ce in the electrocatalysis of EtOH was investigated.

B. Methodology

B.1 Catalyst preparation

The preparation of the 20 wt% Pt deposited on Cerium Oxide (ceria) support was synthesized by using a previously published methodology by Cheung *et. al.*[13] Briefly, 30 mg ceria (NRs or NPs) was sonicated in 9 mL of ethanol and 6 mL of glacial acetic acid for 30 min. Next, 15.12 mg of platinum acetylacetonate was added to the mixture and sonicated for 30 min and then heating with stirring at 100° C until dry. The dry product was finally activated at 400° C in nitrogen at 1.0 Torr for 30 min.

B.2 Experimental setup for XAFS analysis:

X-ray Absorption Spectroscopy (XAFS) was carried out using the beam line X18A at the National Synchrotron Light Source (NSLS) of Brookhaven National Laboratory (BNL). The Pt L_3 edge (11564 eV) was measured for 20% Pt/ceria NR, 20% Pt/ceria NP, and 20% Pt Vulcan sample in the transmission mode. The data acquisition setup consisted of three 12" ionization chamber detectors: Incidence (I_0) Transmittance (I_T) and Reference (I_{Ref}) detector. For Pt L_3 edge, 100% N_2 was used in the I_0 chamber while Ar was used in the I_T and I_{ref} chambers.

The catalysts were mounted in the electrochemical cell for *in-situ* XAFS measurement. Briefly, a catalyst paste was made by mixing 20 mg of catalyst with 3 drops of the 0.1 M KOH solution. Afterwards the catalyst paste was pressed on a carbon cloth and mounted on the electrochemical cell that was used for the *in-situ* analysis.[14] (Figure 1) *In-situ* XAFS measurements were performed of each catalysts with and without 0.5 M ethanol in 0.1 M KOH at applied potentials of -0.680 V, -0.350 V, 0.000 V, and 0.300 V vs. Ag/AgCl. All measurements were done at room temperature.

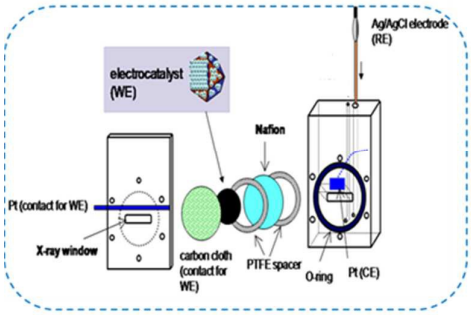

Figure 1. Schematic representation of the in-situ XAFS electrochemical cell used in this study (used with permission from Elsevier).[14]

The XAFS data were analyzed by the Demeter suite of XAS Data Analysis[15]: Normalized absorption coefficients were obtained with the Athena software and EXAFS theoretical fittings were done with the Artemis Software. The coordination numbers were calculated using the passive electron factor (S_0^2) obtained from a platinum foil reference. Bond distance was calculated assuming all bond distortions were proportional to a constant number in order to reduce fitting parameters. For the purpose of this study, white line intensities were normalized by the following equation:

$$WL_{norm} = \frac{WL - WL_{min}}{WL_{max} - WL_{min}} \quad (1)$$

where WL_{norm} is the normalized white line intensity, WL is the non-normalized white line intensity and WL_{min} and WL_{max} are the minimum and maximum white line intensity in the data set, respectively. Each data set of each catalyst was performed in both presence and absence of ethanol. This normalization serves to measure the relative vacancies in the platinum d-band between different samples in under different conditions. Values of WL_{norm} range from 0 to 1. The value of 1 represents the sample with the most vacancies (highest relative electron density), and the value of 0 represents the sample with the least vacancies (lowest relative electron density).

B.3 Electrochemical Experiments

B.3.1 Electrode preparation

A 0.1 M KOH (Sigma Aldrich, 99.99% trace metal basis, company address) and a 0.5 M H_2SO_4 (Fisher, 93-97% Optima, company address) solution were prepared. The ceria containing catalyst inks were prepared by mixing the as-prepared catalysts or Platinum nominally 20% on Vulcan XC-72 (Alfa Aesar) with 200 µL of water per mg of catalyst. The ink and metal concentration were chosen in order to obtain higher signal to noise ratio in the in-situ EXAFS measurements. The mixtures were placed on and ultra-sonic reactor for 2 minutes in order to create a suspension.

Glassy carbon (GC) electrodes (BASi, company address) were prepared by first polishing until a glassy finish was obtained and then were subjected to 2 cycles of a cyclic voltammetry (Biologic Potentiostat HPC-803) in KOH 0.1 M from -0.1 V to 1.1 V vs. Ag/AgCl at 100 mV/s in order to clean the surface and to ensure that resistance and capacitance were within working conditions. The electrodes were dried with nitrogen before placing a 10 µL drop of catalyst ink in the GC surface and were dried in an oven at 115 °C for 3 minutes.

The modified electrodes were submerged in 0.5 M H_2SO_4 solution and held at 0.0 V vs Ag/AgCl with a Pt wire counter electrode for 20 minutes while bubbling the solution with CO. After 20 minutes, the solution was changed and a cyclic voltammogram was taken from -0.200 V to 1.200 V vs Ag/AgCl at 100 mV/s. This was done in order to ensure that the synthesized catalyst had a clean surface. The electrodes were then changed to a 0.1 M KOH solution where the platinum surface area was determined by the hydrogen adsorption/desorption region[16]. It is important to note that every current density reported in this study corresponds to real platinum surface area a not to total real electrode surface area. All potentials in this study are quoted vs. Ag/AgCl.

B.3.2 Ethanol Potentiodynamic and Potentiostatic curves

A 0.5 M ethanol (Aldrich, 99.5%) solution was prepared in 0.1 M KOH (Sigma Aldrich, 99.99% trace metal basis). The clean electrodes were submerged in EtOH and allowed to reach

equilibrium before subjecting them to a linear sweep voltammetry at 1 mV/s from -0.900 to 0.500 V vs Ag/AgCl. Cyclic voltammetry experiments were done from -0.900 V to 0.500 V vs Ag/AgCl at 100 mV/s. New electrodes were prepared and cleaned as described above before performing any studies. For potentiostatic experiments, the electrodes were placed in an EtOH solution, the working electrode was held a -0.450 V for 30 minutes and the current response was measured.

C. Results and Discussions

C.1 Electrochemical Experiments

C.1.1 Cyclic Voltammetry Ethanol 0.5M in KOH 0.1M

Linear Sweep Voltammetry at a scan rate of 1 mV/s was conducted in order to probe the reaction rate of the ethanol oxidation reaction with negligible contribution from capacitance. Figure 2 shows that Pt/ceria NR has the highest current density and thus, faster kinetics for ethanol oxidation[17]. Interestingly, the Pt/ceria NP catalyst shows the lowest overpotential towards ethanol oxidation in alkaline media.

We propose that the potential region from -0.600 V to -0.450 V vs Ag/AgCl corresponds to the C_1 pathway described by Koper et al.[18] and the major products expected to be formed in this region are CO_{ads} and other adsorbed C_1 species[18-20]. These species, specifically the adsorbed C_1 species, are considered to poison the catalyst surface and consequently hinder Pt active sites[18-22]. The Pt/ceria NP catalyst shows higher current density in this region which means it produces higher amounts of these poisoning intermediates. We infer that the reduced oxidation current in the Pt/ ceria NP catalyst when compared to the Pt/ ceria NR catalyst is due to the increased catalytic activity in creating these intermediate poisoning species.

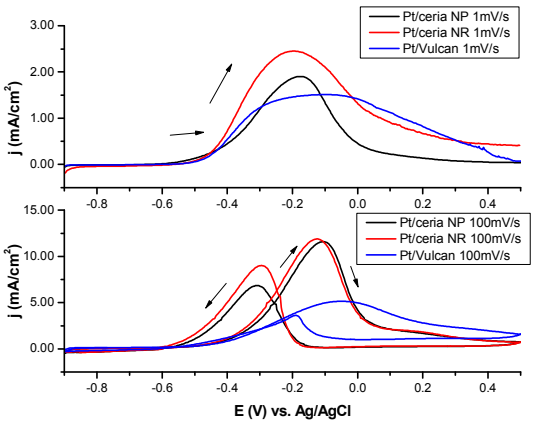

Figure 2. Linear Sweep Voltammetry (v =1 mV/s) and Cyclic Voltammetry (v =100 mV/s) of both ceria supported platinum catalysts and Pt/Vulcan in 0.5 M Ethanol in 0.1 M KOH.

Cyclic voltammograms were taken at fast scan rates in order to prove that lower currents in the Pt/ceria NP catalysts were due to adsorbed poisoning species. At a scan rate of 100 mV/s, we can see that the ceria supported catalysts have similar onset potential and very similar peak current densities. This implies that the C_1 reaction pathway is now virtually inaccessible for all three tested catalysts (because the poisoning rate is equal in all catalysts) and the mechanism that favors intermediates with two carbons is favored. Both ceria supported catalysts show higher current densities and lower overpotentials; both observations are attributed to the high capacity of the ceria support to donate OH_{ads} to the Pt surface.[13, 23-25]

C.1.2 Chronoamperometry

Chronoamperometric studies were performed at -0.450 V vs. Ag/AgCl. Figure 3 shows that the Pt/ceria NP catalysts showed the highest current response, followed by Pt/ ceria NR and Pt/Vulcan. Pt/ceria NP, Pt/ceria NR and Pt/Vulcan showed similar percent change of current with 84%, 82% and 80% respectively which shows that after 30 minutes, the poisoning rate is similar in all three tested catalysts.

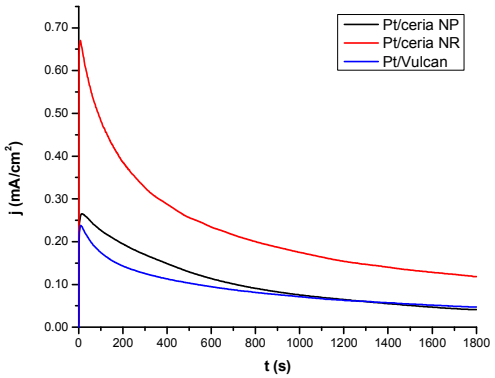

Figure 3. Chronoamperometry of both ceria supported platinum catalysts and Pt/Vulcan in 0.5 M Ethanol in 0.1 M KOH at -0.450 V vs. Ag/AgCl for 30 minutes.

All three current transients show a peak in the first 20 seconds of the potentiostatic study. This peak may be attributed to either an Eley-Rideal (E-R) mechanism or a non-competitive Langmuir Hinshelwood (L-H) mechanism[26]. The fact that the Pt/ceria NP catalyst takes the most time to reach the peak current lends credence to the hypothesis that there is an increased oxidation rate in the beginning due to the C_1 mechanism.

C.2 Ex-situ XRD, PDF and TEM

Ex-situ XRD (Figure 4) and Pair Distribution Function (PDF) analysis (Figure 5) show that we cannot conclude that there is direct intercalation between the CeO_2 and Pt lattices. PDF analysis shows that both Pt/ceria NP and Pt/ceria NR are the result of an addition of independent platinum and CeO_2 lattices. XRD also corroborate that there are no interactions detected between the ceria and platinum crystals. Even though we cannot conclusively state that there is a bonding interaction between ceria and platinum (i.e. no Pt-O-Ce or Pt-Ce bond formation), we must account for the fact that XAFS, XRD and PDF are all bulk sensitive techniques. Since the size of the platinum nanoparticles range from 13 ± 2 nm to 17.0 ± 0.2 nm in diameter, it is possible that some interactions are being

formed in the surface interface between platinum and ceria but some may remain undetected using these techniques.

TEM images are displayed in Figure 6. Platinum nanoparticles were observed to have a wide size distribution in both catalysts along with low dispersion (A, B). This is in accordance to electrochemical studies where the current measured were low. Indeed, the electrochemical measurements in Section 3.1 show that the platinum in the synthesized catalysts do not show the same catalytic activity. This indicates that there are either small electronic or structural changes on the platinum surface, which is confirmed via our *in-situ* XAFS studies.

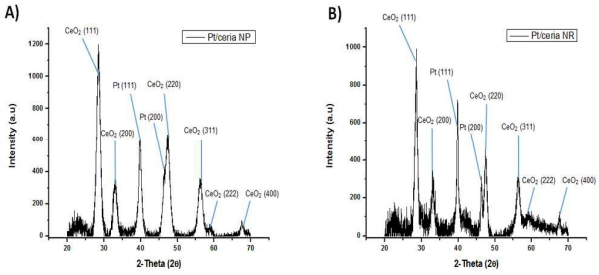

Figure 4. *Ex-situ* XRD spectra of both ceria supported platinum catalysts. Platinum nanoparticles in Pt/ceriaNP and Pt/ceria NR where found to have a diameter of 13 ± 2 nm and 17.1 ± 0.2 nm respectively via the Halder-Wagner Method.

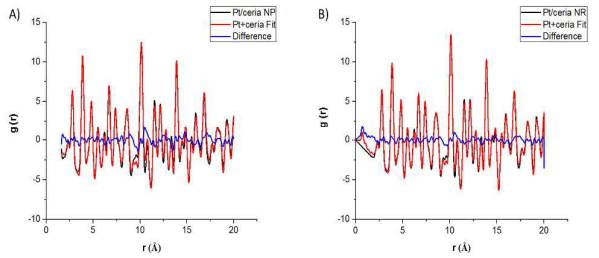

Figure 5. *Ex-situ* PDF analysis of both ceria supported platinum catalysts. The fittings were done with separate theoretical metallic Pt and CeO_2 crystallite structures. The black lines represent the experimental results, the red lines the theoretical fitting and the blue lines the difference between experimental and theoretical intensities.

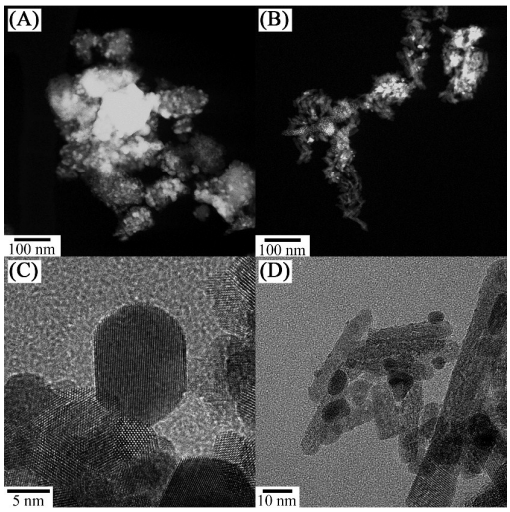

Figure 6. STEM and TEM images showing (A, C) Pt/ceria NPs and (B, D) Pt/ceria NRs.

C.3 In-situ XAFS Studies

Even though XAFS is a bulk sensitive technique and electrochemical phenomena is completely surface sensitive, some information pertaining the system was obtained. The results of the in-situ XAFS studies are summarized in Figure 7. The first shell Pt coordination number in bulk platinum is 12[27] and since the platinum nanoparticles have a large diameter, a decrease in coordination number should be due to a decrease in Pt-Pt bonds and not due to size[27]. It follows that when the coordination number is less than 12, the remaining bonds are filled with another atom. The synthesized catalysts were tested in KOH solutions and EtOH solutions so it is assumed that platinum is filling the remaining vacancies with either carbon or oxygen bonds.

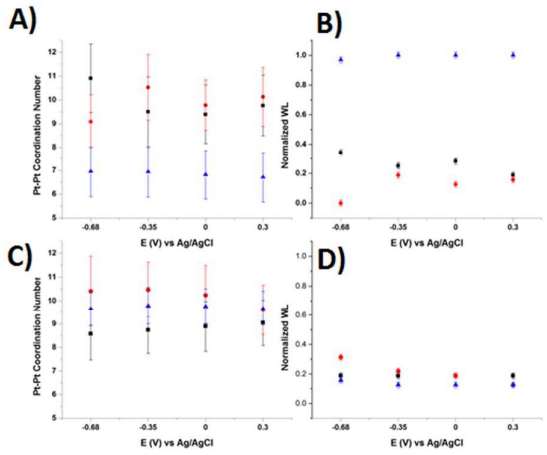

Figure 7. Pt coordination number and Normalized White Line Intensity as calculated in section 2.2 as a function of applied potential in KOH (A,B) and EtOH (C,D). The legend is as follows: Pt/ceria NP (Black Squares), Pt/ceria NR (Red Circles) and Pt/Vulcan (Blue Triangles).

Since oxygen and carbon have very similar atomic number, EXAFS fittings cannot differentiate between them. In

order to overcome this shortcoming, White Line (WL) intensities were normalized and represented in Figures 7B and 7D. High white line intensities correspond to a high amount of vacancies in the d-band[28]. We measured the white line intensities of all catalysts at every potential and normalized them so that 1 corresponds to the highest WL intensity (the species with the *d*-band with the least electron density) and 0 to the lowest (the species with the *d*-band with the most electron density).

The synthesized catalysts showed increased first shell Pt coordination number when compared to the Pt/Vulcan standard in KOH at every potential tested. The high coordination allows us to conclude that the ceria supported catalysts are more resistant to oxidation than the Pt/Vulcan counterpart. Normalized white line intensities also show that both synthesized catalysts have more electron density in their d-band than Pt/Vulcan, also confirming that the synthesized catalysts are harder to oxidize. There have been previous in-situ XAFS studies[29] that showed that this resistance to oxidation is due to charge transfer from the ceria support. Interestingly, the morphology of the ceria support seems to play an important role in charge transfer because white line intensities in the ceria NR support are smaller than on ceria NP. We postulate that this increased charge transfer contribution can be attributed to the fact that the ceria nanorods provide a flatter support where the Pt nanoparticles can grow with more surface area overlap.

The *in-situ* XAFS studies in EtOH showed that there are several key aspects that help explain the observed electrochemical performance of each catalyst. The Pt/Vulcan used as a control shows an increase in first shell Pt-Pt coordination number which indicates that in an EtOH solution it is more favorable thermodynamically for platinum to bond with another platinum atom than to another atom. This contrasts with what is represented in Figure 7A where platinum forms almost half of its bonds with oxygen. Figure 7D allows us to conclude that the identity of the atom that is bonded to platinum in the EtOH solution is carbon, not oxygen (from hydroxide species, water or EtOH) because there is a higher amount of electron density on the platinum d-band than that which was observed when there was only oxygen present. The normalized white line intensity of the Pt/Vulcan support is much smaller in the EtOH solution indicating that there are fewer vacancies on its d-band. An electronegative atom like oxygen would take electron density away from the platinum, making the normalized white line intensity higher (as in Figure 7B).

The first shell coordination number between the two synthesized catalysts did not present any statistically significant variation in the XAFS experiments in EtOH. For this reason, all of the conclusions must be drawn from their variations in normalized white line intensity. The Pt/ceria NP catalyst showed a decrease in normalized white line intensity at every potential. The decrease in white line intensity is due to the fact that oxygen must now compete with carbon in order to form bonds with the platinum surface. The decreased electronegativity of carbon with respect to oxygen causes fewer vacancies in the *d*-band and thus a decrease in white line intensity. Interestingly, the Pt/ceria NR catalyst showed the opposite trend when comparing normalized white line intensities between the KOH and EtOH solutions. We propose that this increase in white line intensity in the EtOH solution when compared to the KOH solution is due to the increased charge transfer efficiency between Pt and the ceria support. The XANES results in the KOH solution show that, since the platinum *d*-band is kept relatively full, the Pt surface is less electrophilic and this decreases the efficiency of the nucleophilic hydroxide adsorption. When ethanol is added to the solution, the increased nucleophilicity of the platinum surface due to ceria charge transfer facilitates the formation of a bond between the electron rich platinum and the electron deficient carbon in ethanol. Once this bond is formed, the carbon will take electrons from the platinum d-band. This will decrease the overall electron density increase the white line intensity. White line intensities in KOH show that the ceria NR catalyst has the least amount of hydroxide in its surface so when EtOH is added, more electron-withdrawing species bind to the surface, thus increasing its white line intensity. This contrasts with the ceria NP catalyst where hydroxide species are exchanged with EtOH and the comparatively lower electronegativity of carbon versus oxygen decreases the white line intensity.

The increased nucleophilicity of platinum in the ceria supported catalysts could explain their increased catalytic activity in Figure 2. The fact that the characteristic hydrogen underpotential deposition region of platinum is absent in the cyclic voltammograms is proof that ethanol can bind to the platinum surface at negative potentials.[21] In the potential region between -0.680 V and -0.350 V vs Ag/Cl, the ceria NR catalyst shows higher current density which correlates with more efficient ethanol bond formation due to ceria charge transfer.

Conclusions

Pt and CeO_2 catalysts with either NP or NR morphologies were prepared and characterized both physically and electrochemically. As previously reported [13, 23, 24], potentiodynamic experiments showed that the ceria support increased the catalytic activity of the Pt nanoparticles in the EOR when compared to commercial Pt/Vulcan. This has previously been attributed to the fact that metallic platinum can exist at more positive potentials than usual due to the ceria support.[29] In this study we show that the ceria support donates electron density to the platinum *d*-band. This decreases platinum electrophilicity and diminishes hydroxide adsorption on Pt at all tested potential when compared to Pt/Vulcan. The increased platinum nucleophilicity imparted by the ceria support aids in forming the bond between platinum and the electrophilic carbon in ethanol and could help explain the synthesized catalysts' improved electrochemical activity. We also show that the morphology of the catalyst plays an important role in charge transfer; we propose that the greater the surface area overlapped between platinum and ceria, the more efficient the charge transfer, as evidenced by white line intensities.

Acknowledgements

Use of the National Synchrotron Light Source, Brookhaven National Laboratory, was supported by the U.S. Department of Energy, Office of Science, Office of Basic Energy Sciences, under Contract No. DE-AC02-98CH10886. The authors would also like to acknowledge Steven N. Ehrlich (NSLS), Syed Khalid (NSLS) and Nebojša Marinković (NSLS) for their help with experimental setup at Beamline X-18A. This work had financial support of NASA-MIRO Grant No. NNX10AQ17A. Financial support of the NSF-NSEC Center for Hierarchical Manufacturing, Grant No. CHM-CMMI-0531171, is also gratefully acknowledged.

Notes and references

1. H. D. Abruña, *Journal of Chemical Education*, 2013, **90**, 1411-1413.
2. E. Antolini, *Materials Chemistry and Physics*, 2003, **78**, 563-573.
3. J. P. I. de Souza, S. L. Queiroz, K. Bergamaski, E. R. Gonzalez and F. C. Nart, *The Journal of Physical Chemistry B*, 2002, **106**, 9825-9830.
4. Z. X. Liang, T. S. Zhao, J. B. Xu and L. D. Zhu, *Electrochimica Acta*, 2009, **54**, 2203-2208.
5. Y. Chen, L. Zhuang and J. Lu, *Chinese Journal of Catalysis*, 2007, **28**, 870-874.
6. W. Du, N. A. Deskins, D. Su and X. Teng, *ACS Catalysis*, 2012, **2**, 1226-1231.
7. W. P. Zhou, S. Axnanda, M. G. White and R. R. Adzic, *Abstracts of Papers of the American Chemical Society*, 2011, **242**, 1.
8. J. W. Magee, W.-P. Zhou and M. G. White, *Applied Catalysis B: Environmental*, 2014, **152–153**, 397-402.
9. J. Melke, A. Schoekel, D. Dixon, C. Cremers, D. E. Ramaker and C. Roth, *The Journal of Physical Chemistry C*, 2010, **114**, 5914-5925.
10. C. L. Campos, C. Roldán, M. Aponte, Y. Ishikawa and C. R. Cabrera, *Journal of Electroanalytical Chemistry*, 2005, **581**, 206-215.
11. M. Shen, L. Lv, J. Wang, J. Zhu, Y. Huang and J. Wang, *Chemical Engineering Journal*, 2014, **255**, 40-48.
12. R. Guzmán-Blas, C. L. Menéndez, C. A. Vélez, E. Fachini, A. Johnston-Peck, S. D. Senanayake, D. Stacchiola, K. Sasaki and C. R. Cabrera, *Journal*, 2013, **4**, 1-9.
13. Y. Zhou, C. L. Menendez, M. J. F. Guinel, E. C. Needels, I. Gonzalez-Gonzalez, D. L. Jackson, N. J. Lawrence, C. R. Cabrera and C. L. Cheung, *Rsc Advances*, 2014, **4**, 1270-1275.
14. K. Sasaki, J. X. Wang, H. Naohara, N. Marinkovic, K. More, H. Inada and R. R. Adzic, *Electrochimica Acta*, 2010, **55**, 2645-2652.
15. B. Ravel and M. Newville, *Journal of Synchrotron Radiation*, 2005, **12**, 537-541.
16. J. Corchado-García and C. Cabrera, *Electrocatalysis*, 2014, DOI: 10.1007/s12678-014-0207-0, 1-6.
17. A. J. Bard and L. R. Faulkner, *Electrochemical Methods: Fundamentals and Applications*, Wiley, 2000.
18. S. C. S. Lai and M. T. M. Koper, *Physical Chemistry Chemical Physics*, 2009, **11**, 10446-10456.
19. J. S. Spendelow and A. Wieckowski, *Physical Chemistry Chemical Physics*, 2007, **9**, 2654-2675.
20. F. Colmati, G. Tremiliosi-Filho, E. R. Gonzalez, A. Berna, E. Herrero and J. M. Feliu, *Physical Chemistry Chemical Physics*, 2009, **11**, 9114-9123.
21. R. B. Kutz, B. Braunschweig, P. Mukherjee, R. L. Behrens, D. D. Dlott and A. Wieckowski, *Journal of Catalysis*, 2011, **278**, 181-188.
22. C. Xu, P. k. Shen and Y. Liu, *Journal of Power Sources*, 2007, **164**, 527-531.
23. C. Xu, R. Zeng, P. K. Shen and Z. Wei, *Electrochimica Acta*, 2005, **51**, 1031-1035.
24. C. Xu and P. K. Shen, *Journal of Power Sources*, 2005, **142**, 27-29.
25. R. T. Kinch, C. R. Cabrera and Y. Ishikawa, *The Journal of Physical Chemistry C*, 2009, **113**, 9239-9250.
26. J. S. Spendelow, J. D. Goodpaster, P. J. A. Kenis and A. Wieckowski, *The Journal of Physical Chemistry B*, 2006, **110**, 9545-9555.
27. A. Jentys, *Physical Chemistry Chemical Physics*, 1999, **1**, 4059-4063.
28. A. J. Berry, H. S. C. O'Neill, K. D. Jayasuriya, S. J. Campbell and G. J. Foran, *American Mineralogist*, 2003, **88**, 967-977.
29. T. Masuda, H. Fukumitsu, K. Fugane, H. Togasaki, D. Matsumura, K. Tamura, Y. Nishihata, H. Yoshikawa, K. Kobayashi, T. Mori and K. Uosaki, *The Journal of Physical Chemistry C*, 2012, **116**, 10098-10102.